The Galactic Center Region Gamma Ray Excess from A Supersymmetric Leptophilic Higgs Model

Gardner Marshall* and Reinard Primulando†

Particle Theory Group, Department of Physics,

College of William and Mary, Williamsburg, VA 23187-8795

(Dated: February 2011)

Abstract

In a recent paper by Hooper and Goodenough, data from the Fermi Gamma Ray Telescope was analyzed and an excess of gamma rays was claimed to be found in the emission spectrum from the Galactic Center Region. Hooper and Goodenough suggest that the claimed excess can be well explained by 7-10 GeV annihilating dark matter with a power law density profile if the dark matter annihilates predominantly to tau pairs. In this paper we present such a dark matter model by extending the MSSM to include four Higgs doublets and one scalar singlet. A $\mathbb{Z}_2$ symmetry is imposed that enforces a Yukawa structure so that the up quarks, down quarks, and leptons each receive mass from a distinct doublet. This leads to an enhanced coupling of scalars to leptons and allows the model to naturally achieve the required phenomenology in order to explain the gamma ray excess. Our model yields the correct dark matter thermal relic density and avoids collider bounds from measurements of the Z width as well as direct production at LEP.

*grmarshall@email.wm.edu

†rprimulando@email.wm.edu

I. INTRODUCTION

Recently, Hooper and Goodenough examined the first two years of Fermi Gamma Ray Space Telescope (FGST) data from the inner 10° around the Galactic Center [1]. They found that the gamma ray emissions coming from between 1.25° and 10° of the Galactic Center is consistent with what is expected from known emission mechanisms such as cosmic rays colliding with gas to produce subsequently decaying pions, inverse Compton scattering of cosmic ray electrons, and known gamma ray point sources. In order to model the gamma ray background within 2° of the Galactic Center, Hooper and Goodenough model the emission of the Galactic black hole Sgr A* as a power-law extrapolated from higher energy HESS observations. Comparing the FGST measurements to this background, Hooper and Goodenough found that it agrees very well with FGST data between $1.25° - 2°$ but found an excess in the observed gamma ray intensity within 1.25°. It has been pointed out by Ref. [2] however, that a simple power-law extrapolation of HESS data may understate the flux of the central point source Sgr A* as the slope of its spectrum may deviate from the constant HESS results below an energy of 100 GeV.

The authors of Ref. [1] showed that the increased gamma ray emissions are well described by annihilating dark matter that has a cusped halo profile ($\rho \propto r^{-\gamma}$, with $\gamma = 1.18$ to 1.33) provided that the dark matter satisfies three basic conditions. The conditions required of the dark matter are 1) that it have a mass between $7 - 10$ GeV, 2) that it annihilate into τ-pairs most of the time, but into hadronic channels $15 - 40\%$ of the time, and 3) that its total annihilation cross section yield a thermal average within the range $\langle \sigma v \rangle = 4.6 \times 10^{-27} - 5.3 \times 10^{-26}$ cm^3/s. It should be noted that the results of Hooper and Goodenough are controversial, and the Fermi-LAT collaboration itself has not yet published official results. In addition, other background related explanations for the gamma ray excess have been proposed such as the existence of a pulsar near the Galactic Center [3]. In this paper we proceed with the assumption that the analysis of Hooper and Goodenough is correct. The astrophysical and particle physics implications of this finding are discussed in Refs. [4, 5].

In this paper we construct a dark matter model satisfying the above conditions by adding a singlet to the supersymmetric leptophilic Higgs model (SLHM) [6]. In the SLHM the up quarks, down quarks, and leptons, each receive mass from a separate Higgs doublet. For our purposes, the salient characteristic of the SLHM is that it endows the leptons with an

enhanced coupling to one of the scalars. This provides a natural mechanism for dark matter particles to annihilate predominantly into τ-pairs. This model of dark matter is able to successfully account for the FGST observations, yields the correct relic density, and evades relevant collider bounds such as measurements of the Z width and direct production at LEP. The idea of a leptophilic Higgs has been studied as a possible explanation for the $e^{\pm}$ excess observed by PAMELA and ATIC in Ref. [7]. However, this entails a 100 GeV - 1 TeV dark matter particle, while our model requires a light, $\mathcal{O}(10)$ GeV dark matter particle. There also exist some other models that can explain the Galactic Center gamma ray excess [8].

In addition to explaining the FGST observations, such a model of light dark matter is also capable of describing observations by the CoGeNT [9] and DAMA collaborations [10]. CoGeNT has recently reported direct detection signals that hint at the presence of $\mathcal{O}(10)$ GeV dark matter compatible with the light dark matter interpretation of DAMA's annual event rate modulation. Ref. [11] showed that dark matter with a mass between $7-8$ GeV that has a spin independent cross section approximately between $\sigma_{SI} = 1 \times 10^{-40} - 3 \times 10^{-40}$ cm^2 is consistent with both CoGeNT and DAMA signals. Although the XENON [12] and CDMS [13] collaborations challenge this report, Ref. [5] has pointed out that "zero-charge" background events lie in the signal region. The authors suggest that the bound could possibly be loosened if a modest uncertainty or systematic error is introduced in the energy scale calibration near the energy threshold. Although our model is able to explain the reported observations of the CoGeNT and DAMA collaborations, it is not dependent upon their validity. By simply moving to another region of parameter space our model can coexist with the absolute refutation of CoGeNT and DAMA while continuing to explain the FGST results and avoiding collider bounds.

Our paper is organized as follows. In Section II we introduce the setup of the model and calculate the mass matrices for the scalars and the neutralinos. In Section III we describe the process by which the dark matter annihilates into Standard model particles and calculate the relevant cross sections for a benchmark point in parameter space. We also show that the resultant relic density is consistent with current cosmological measurements. In Section IV we discuss possible direct detection and in Section V we discuss relevant bounds for this model and show that it is currently viable. Lastly, we conclude with Section VI and summarize the results of the paper.

II. THE MODEL

In this model the quark and lepton content is that of the MSSM. To this we add four Higgs doublets, $\widehat{H}_u$, $\widehat{H}_d$, $\widehat{H}_0$, and $\widehat{H}_\ell$, with weak hypercharge assignment $+1/2$, $-1/2$, $+1/2$, and $-1/2$ respectively. The third Higgs doublet is necessary to achieve a leptonic structure, while the fourth doublet is required for anomaly cancelation. In order to avoid problems with the Z decay width, we introduce a singlet $\widehat{S}$ that acts as $\mathcal{O}(10)$ GeV dark matter. The idea of adding a light singlet to the MSSM to act as dark matter was also considered in [14], while the use of a singlet for other purposes such as solving the μ problem was first developed in [15]. The superpotential is given by

$$\begin{aligned} W = {} & y_u \widehat{U}\widehat{Q}\widehat{H}_u - y_d \widehat{D}\widehat{Q}\widehat{H}_d - y_\ell \widehat{E}\widehat{L}\widehat{H}_\ell + \mu_q \widehat{H}_u\widehat{H}_d + \mu_\ell \widehat{H}_0\widehat{H}_\ell \\ & + \kappa_q \widehat{S}\widehat{H}_u\widehat{H}_d + \kappa_\ell \widehat{S}\widehat{H}_0\widehat{H}_\ell + \lambda_1^2 \widehat{S} + \frac{1}{2}\,\lambda_2 \widehat{S}^2 + \frac{1}{3}\,\kappa_s \widehat{S}^3, \end{aligned} \tag{2.1}$$

where the hats denote superfields. In the superpotential we introduced a $\mathbb{Z}_2$ symmetry under which $\widehat{H}_0$, $\widehat{H}_\ell$ and $\widehat{E}$ are odd while all other fields are even. The symmetry enforces a Yukawa structure in which $\widehat{H}_u$ gives mass to up-type quarks, $\widehat{H}_d$ to down-type quarks, and $\widehat{H}_\ell$ to leptons, while $\widehat{H}_0$ does not couple to the quarks or leptons and is called the inert doublet. It is introduced to ensure anomaly cancellation. The $\mathbb{Z}_2$ symmetry is broken in $V_{\rm soft}$ so that we have: [1]

$$\begin{aligned} V_{\rm soft} = {} & m_u^2|H_u|^2 + m_d^2|H_d|^2 + m_0^2|H_0|^2 + m_\ell^2|H_\ell|^2 + m_s^2|S|^2 \\ & + \Big(\mu_1^2 H_u H_d + \mu_2^2 H_0 H_\ell + \mu_3^2 H_u H_\ell + \mu_4^2 H_0 H_d \\ & + \mu_a S H_u H_d + \mu_b S H_0 H_\ell + \mu_c S H_u H_\ell + \mu_d S H_0 H_d \\ & + m_{u0}^2 H_u^\dagger H_0 + m_{d\ell}^2 H_d^\dagger H_\ell + t^3 S + b_s^2 S^2 + a_s S^3 + \text{h.c.}\Big). \end{aligned} \tag{2.2}$$

The breaking of the $\mathbb{Z}_2$ symmetry is discussed in greater detail in Appendix A. The Higgs sector potential is given by $V = V_D + V_F + V_{\rm soft}$. Letting σ^a denote the Pauli matrices for $a = 1, 2, 3$, the D-term is simply

$$\begin{aligned} V_D = {} & \frac{g^2}{8} \sum_a \left| H_u^\dagger \sigma^a H_u + H_d^\dagger \sigma^a H_d + H_0^\dagger \sigma^a H_0 + H_\ell^\dagger \sigma^a H_\ell \right|^2 \\ & + \frac{g'^2}{8} \left| |H_u|^2 - |H_d|^2 + |H_0|^2 - |H_\ell|^2 \right|^2, \end{aligned} \tag{2.3}$$

[1] In Ref. [6] the soft breaking terms $m_{u0}^2 H_u^\dagger H_0 + m_{d\ell}^2 H_d^\dagger H_\ell + \text{h.c.}$ were omitted.

where g and g' are the $SU(2)$ and $U(1)$ gauge couplings respectively. The F-term and $V_{\rm soft}$ combine with the D-term to yield the following potential

$$\begin{aligned}
V = {} & \big(\mu_q^2 + m_u^2\big)|H_u|^2 + \big(\mu_q^2 + m_d^2\big)|H_d|^2 + \big(\mu_\ell^2 + m_0^2\big)|H_0|^2 + \big(\mu_\ell^2 + m_\ell^2\big)|H_\ell|^2 \\
& + \Big[\big(\mu_1^2 + \kappa_q\lambda_1^2\big)H_uH_d + \big(\mu_2^2 + \kappa_\ell\lambda_1^2\big)H_0H_\ell + \mu_3^2 H_uH_\ell + \mu_4^2 H_0H_d + \text{h.c.}\Big] \\
& + \Big|\kappa_q H_uH_d + \kappa_\ell H_0H_\ell\Big|^2 + \Big(m_{u0}^2 H_u^\dagger H_0 + m_{d\ell}^2 H_d^\dagger H_\ell + \text{h.c.}\Big) + \big(m_s^2 + \lambda_2^2\big)|S|^2 \\
& + \Big[\big(t^3 + \lambda_1^2\lambda_2\big)S + \big(b_s^2 + \kappa_s\lambda_2^2\big)S^2 + a_s S^3 + \text{h.c.}\Big] + \kappa_s\lambda_2|S|^2\big(S + S^*\big) + \kappa_s^2|S|^4 \\
& + \Big[\mu_a\big(H_uH_d\big)S + \mu_b\big(H_0H_\ell\big)S + \mu_c\big(H_uH_\ell\big)S + \mu_d\big(H_0H_d\big)S + \text{h.c.}\Big] \\
& + \Big\{\lambda_2\Big[\kappa_q\big(H_uH_d\big) + \kappa_\ell\big(H_0H_\ell\big)\Big]S^* + \kappa_s\Big[\kappa_q\big(H_uH_d\big) + \kappa_\ell\big(H_0H_\ell\big)\Big](S^2)^* + \text{h.c.}\Big\} \\
& + \Big\{\kappa_q\mu_q\Big(|H_u|^2 + |H_d|^2\Big) + \kappa_\ell\mu_\ell\Big(|H_0|^2 + |H_\ell|^2\Big)\Big\}\big(S + S^*\big) \\
& + \kappa_q^2\Big(|H_u|^2 + |H_d|^2\Big)|S|^2 + \kappa_\ell^2\Big(|H_0|^2 + |H_\ell|^2\Big)|S|^2 + V_D.
\end{aligned} \tag{2.4}$$

The singlet S acquires the vev $\langle S\rangle = v_s/\sqrt{2}$ while the Higgs doublets acquire the vevs:

$$\langle H_u\rangle = \frac{1}{\sqrt{2}}\begin{pmatrix} 0 \\ v_u \end{pmatrix}, \quad \langle H_d\rangle = \frac{1}{\sqrt{2}}\begin{pmatrix} v_d \\ 0 \end{pmatrix}, \langle H_0\rangle = \frac{1}{\sqrt{2}}\begin{pmatrix} 0 \\ v_0 \end{pmatrix}, \quad \langle H_\ell\rangle = \frac{1}{\sqrt{2}}\begin{pmatrix} v_\ell \\ 0 \end{pmatrix}. \tag{2.5}$$

Letting $v_{\rm ew}^2 = v_u^2 + v_d^2 + v_0^2 + v_\ell^2$ so that $v_{\rm ew}^2 = 4M_Z^2/(g^2 + g'^2) \approx (246\text{ GeV})^2$, we define the mixing angles α, β, and β_ℓ by the relations $\tan\beta = v_u/v_d$, $\tan\beta_\ell = v_0/v_\ell$, and $\tan^2\alpha = (v_u^2 + v_d^2)/(v_0^2 + v_\ell^2)$. These definitions lead to the following parameterization of the Higgs vevs:

$$\begin{aligned}
v_u &= v_{\rm ew}\sin\alpha\sin\beta, \quad & v_d &= v_{\rm ew}\sin\alpha\cos\beta, \\
v_0 &= v_{\rm ew}\cos\alpha\sin\beta_\ell, \quad & v_\ell &= v_{\rm ew}\cos\alpha\cos\beta_\ell.
\end{aligned} \tag{2.6}$$

In order to avoid increasing the Z width or violating other known bounds, we want the light dark matter to separate from the other neutralinos and be mostly singlino $\tilde{s}$, the fermionic component of the singlet $\widehat{S}$. This is accomplished by taking the parameters κ_q and κ_ℓ to be small, which eliminates most of the mixing between the singlino and the Higgsinos [see Eq. (2.10)]. It can then be easily arranged to have the singlino be the lightest of the neutralinos. A possible mechanism for explaining the small size of κ_q and κ_ℓ is discussed in Appendix A. Small values of κ_q and κ_ℓ also leads to reduced mixing between the scalar singlet and the Higgs doublets as can be seen from Eq. (2.4). A small amount of mixing is of course required since we desire the lightest scalar, which is mostly singlet, to couple

to τ-pairs in order for the dark matter to annihilate to $\tau^+\tau^-$ and other Standard Model particles. This mixing is generated by the soft supersymmetry-breaking parameters μ_a, μ_b, μ_c, and μ_d.

It is sufficient for κ_q and κ_ℓ to be $\mathcal{O}(10^{-2})$, which is what we use in our numerical calculations (see Table I and II). Though the scalar mass matrices are quite complicated in general, they simplify considerably in the limit of vanishing κ_q and κ_ℓ. The numerical calculations in the sections that follow have been determined using the general matrices, but for compactness we present only the simplified matrices here. In the $\{h_u, h_d, h_0, h_\ell, h_s\}$ basis, the neutral scalar mass matrix is given by

$$M_N^2 = \begin{pmatrix} M^2 & \overrightarrow{m}^2 \\ \overrightarrow{m}^{2\,T} & M_{SS}^2 \end{pmatrix}, \tag{2.7}$$

where the matrix M^2 is given by $M^2 = M^2_{\rm SLHM} + \Delta M_1^2 + \Delta M_2^2$ and the terms $\overrightarrow{m}^2$ and M_{SS} are given by

$$\overrightarrow{m}^{2\,T} = -\frac{1}{\sqrt{2}}\left(\mu_a v_d + \mu_c v_\ell,\ \mu_a v_u + \mu_d v_0,\ \mu_b v_\ell + \mu_d v_d,\ \mu_b v_0 + \mu_c v_u\right)$$

and

$$M_{SS}^2 = \frac{3\big(a_s + \kappa_s\lambda_2\big)v_s^2 + 2\sqrt{2}\kappa_s^2 v_s^3 - 2t^3 - 2\lambda_1^2\lambda_2 + \big(\mu_a v_u v_d + \mu_b v_0 v_\ell + \mu_c v_u v_\ell + \mu_d v_0 v_d\big)}{\sqrt{2}\, v_s}.$$

The matrix $M^2_{\rm SLHM}$ is the neutral scalar mass matrix from the ordinary SLHM, which can be found in [6], while the matrices ΔM_1^2 and ΔM_2^2 are given by

$$\Delta M_1^2 = \begin{pmatrix} -m_{u0}^2\frac{v_0}{v_u} & 0 & m_{u0}^2 & 0 \\ 0 & -m_{d\ell}^2\frac{v_\ell}{v_d} & 0 & m_{d\ell}^2 \\ m_{u0}^2 & 0 & -m_{u0}^2\frac{v_u}{v_0} & 0 \\ 0 & m_{d\ell}^2 & 0 & -m_{d\ell}^2\frac{v_d}{v_\ell} \end{pmatrix},$$

and

$$\Delta M_2^2 = \frac{1}{\sqrt{2}}\begin{pmatrix} \frac{v_s}{v_u}\left(\mu_a v_d + \mu_c v_\ell\right) & -v_s\mu_a & 0 & -v_s\mu_c \\ -v_s\mu_a & \frac{v_s}{v_d}\left(\mu_a v_u + \mu_d v_0\right) & -v_s\mu_d & 0 \\ 0 & -v_s\mu_d & \frac{v_s}{v_0}\left(\mu_b v_\ell + \mu_d v_d\right) & -v_s\mu_b \\ -v_s\mu_c & 0 & -v_s\mu_b & \frac{v_s}{v_\ell}\left(\mu_b v_0 + \mu_c v_u\right) \end{pmatrix}.$$

The pseudoscalar mass matrix, in the $\{a_u, a_d, a_0, a_\ell, a_s\}$ basis, is similarly given by

$$M_A^2 = \begin{pmatrix} \widetilde{M}^2 & -\overrightarrow{m}^2 \\ -\,\overrightarrow{m}^{2\,T} & \widetilde{M}^2_{SS} \end{pmatrix}, \tag{2.8}$$

where $\widetilde{M}^2 = \widetilde{M}^2_{\rm SLHM} + \Delta M_1^2 + \Delta\widetilde{M}_2^2$. The matrix $\widetilde{M}^2_{\rm SLHM}$ is the pseudoscalar mass matrix from the ordinary SLHM while $\Delta\widetilde{M}_2^2$ is the matrix obtained from ΔM_2^2 by changing the sign of every off-diagonal entry. Lastly, $\widetilde{M}^2_{SS}$ is given by

$$\begin{aligned}\widetilde{M}^2_{SS} = \frac{1}{\sqrt{2}\,v_s}\Big[&\mu_a v_u v_d + \mu_b v_0 v_\ell + \mu_c v_u v_\ell + \mu_d v_0 v_d - 2\lambda_1^2\lambda_2 \\ &- 2t^3 - \big(9a_s + \kappa_s\lambda_2\big)v_s^2 - 4\sqrt{2}\,(b_s^2 + \kappa_s\lambda_2^2)v_s\Big].\end{aligned}$$

The chargino mass matrix, on the other hand, is rather simple even with nonvanishing κ_q and κ_ℓ. Letting $\tilde{h}_u$, $\tilde{h}_d$, $\tilde{h}_0$, and $\tilde{h}_\ell$ denote the Higgsino gauge eigenstates, the chargino mass matrix, in the $\{\widetilde{W}^+, \tilde{h}_u^+, \tilde{h}_0^+, \widetilde{W}^-, \tilde{h}_d^-, \tilde{h}_\ell^-\}$ basis, is given by

$$M_{\chi^\pm} = \begin{pmatrix} 0 & 0 & 0 & M_2 & gv_d & gv_\ell \\ 0 & 0 & 0 & gv_u & \mu_q + \frac{\kappa_q}{\sqrt{2}}v_s & 0 \\ 0 & 0 & 0 & gv_0 & 0 & \mu_\ell + \frac{\kappa_\ell}{\sqrt{2}}v_s \\ M_2 & gv_u & gv_0 & 0 & 0 & 0 \\ gv_d & \mu_q + \frac{\kappa_q}{\sqrt{2}}v_s & 0 & 0 & 0 & 0 \\ gv_\ell & 0 & \mu_\ell + \frac{\kappa_\ell}{\sqrt{2}}v_s & 0 & 0 & 0 \end{pmatrix}. \tag{2.9}$$

Like the chargino mass matrix, the neutralino mass matrix is simple. The neutralino mass matrix, in the $\{\widetilde{B}^0, \widetilde{W}^0, \tilde{h}_u, \tilde{h}_d, \tilde{h}_0, \tilde{h}_\ell, \tilde{s}\}$ basis, is given by

$$M_\chi = \begin{pmatrix} M_1 & 0 & \frac{1}{2}g'v_u & -\frac{1}{2}g'v_d & \frac{1}{2}g'v_0 & -\frac{1}{2}g'v_\ell & 0 \\ 0 & M_2 & -\frac{1}{2}gv_u & \frac{1}{2}gv_d & -\frac{1}{2}gv_0 & \frac{1}{2}gv_\ell & 0 \\ \frac{1}{2}g'v_u & -\frac{1}{2}gv_u & 0 & \mu_q + \frac{\kappa_q}{\sqrt{2}}v_s & 0 & 0 & \frac{\kappa_q}{\sqrt{2}}v_d \\ -\frac{1}{2}g'v_d & \frac{1}{2}gv_d & \mu_q + \frac{\kappa_q}{\sqrt{2}}v_s & 0 & 0 & 0 & \frac{\kappa_q}{\sqrt{2}}v_u \\ \frac{1}{2}g'v_0 & -\frac{1}{2}gv_0 & 0 & 0 & 0 & \mu_\ell + \frac{\kappa_\ell}{\sqrt{2}}v_s & \frac{\kappa_\ell}{\sqrt{2}}v_\ell \\ -\frac{1}{2}g'v_\ell & \frac{1}{2}gv_\ell & 0 & 0 & \mu_\ell + \frac{\kappa_\ell}{\sqrt{2}}v_s & 0 & \frac{\kappa_\ell}{\sqrt{2}}v_0 \\ 0 & 0 & \frac{\kappa_q}{\sqrt{2}}v_d & \frac{\kappa_q}{\sqrt{2}}v_u & \frac{\kappa_\ell}{\sqrt{2}}v_\ell & \frac{\kappa_\ell}{\sqrt{2}}v_0 & \lambda_2 + \sqrt{2}\,\kappa_s v_s \end{pmatrix}. \tag{2.10}$$

When κ_q and κ_ℓ are small, the singlino part of the above matrix separates from the wino, bino, and higgsinos, and the singlino mass can be well approximated by

$$m_{\chi_1} \approx \lambda_2 + \sqrt{2}\,\kappa_s v_s. \tag{2.11}$$

$\kappa_q = 0.01$	$v_s = 50$ GeV	$\mu_\ell = 125$ GeV	$m_{d\ell}^2 = (100\text{ GeV})^2$	$\mu_b = 200$ GeV
$\kappa_\ell = 0.01$	$v_u = 245.6$ GeV	$\lambda_1^2 = (100\text{ GeV})^2$	$\mu_1^2 = (400\text{ GeV})^2$	$\mu_c = 200$ GeV
$\kappa_s = 0.6$	$v_d = 4.9$ GeV	$\lambda_2 = -35$ GeV	$\mu_2^2 = (200\text{ GeV})^2$	$\mu_d = 200$ GeV
$\tan\alpha = 20$	$v_0 = 12.2$ GeV	$M_1 = 500$ GeV	$\mu_3^2 = (200\text{ GeV})^2$	$t^3 = (60.6\text{ GeV})^3$
$\tan\beta = 50$	$v_\ell = 1.2$ GeV	$M_2 = 500$ GeV	$\mu_4^2 = (400\text{ GeV})^2$	$b_s^2 = (63.4\text{ GeV})^2$
$\tan\beta_l = 10$	$\mu_q = 125$ GeV	$m_{u0}^2 = -(100\text{ GeV})^2$	$\mu_a = 100$ GeV	$a_s = -42.4$ GeV

TABLE I: Benchmark Point A

$\kappa_q = 0.01$	$v_s = 50$ GeV	$\mu_\ell = 125$ GeV	$m_{d\ell}^2 = (100\text{ GeV})^2$	$\mu_b = 200$ GeV
$\kappa_\ell = 0.01$	$v_u = 245.6$ GeV	$\lambda_1^2 = (100\text{ GeV})^2$	$\mu_1^2 = (400\text{ GeV})^2$	$\mu_c = 200$ GeV
$\kappa_s = 0.6$	$v_d = 4.9$ GeV	$\lambda_2 = -35$ GeV	$\mu_2^2 = (200\text{ GeV})^2$	$\mu_d = 200$ GeV
$\tan\alpha = 20$	$v_0 = 12.2$ GeV	$M_1 = 500$ GeV	$\mu_3^2 = (200\text{ GeV})^2$	$t^3 = (55.0\text{ GeV})^3$
$\tan\beta = 50$	$v_\ell = 1.2$ GeV	$M_2 = 500$ GeV	$\mu_4^2 = (400\text{ GeV})^2$	$b_s^2 = (66.3\text{ GeV})^2$
$\tan\beta_l = 10$	$\mu_q = 125$ GeV	$m_{u0}^2 = -(100\text{ GeV})^2$	$\mu_a = 100$ GeV	$a_s = -42.2$ GeV

TABLE II: Benchmark Point B

The $\mathcal{O}(10)$ GeV LSP can be arranged with some tuning of the parameters in order to achieve a cancelation between λ_2 and the product $\kappa_s v_s$ in Eq. (2.11). Though the smallness of κ_q and κ_ℓ is technically unnatural, we remind the reader that a possible mechanism to make them small is discussed in Appendix A.

In the following sections, we calculate the relevant cross sections and quantities of interest using benchmark points A and B, found in Tables I and II respectively. While both of these benchmark points can explain the Galactic Central region gamma ray excess, the spin independent direct detection cross section corresponding to benchmark point A lies within the region favored by CoGeNT and DAMA. In contrast, we will show that benchmark point B satisfies CDMS bounds that exclude CoGeNT and DAMA. Relevant quantities have been calculated for several additional benchmark points as well, and their values are summarized in Table VI of Appendix B.

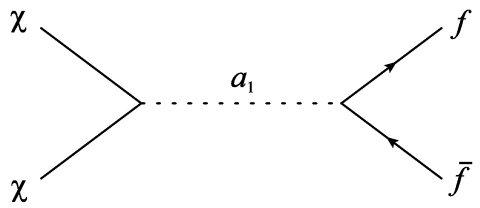

FIG. 1: The dominant diagram of dark matter annihilation into fermions. Here a_1 is the lightest pseudoscalar.

III. ANNIHILATION TO FERMIONS

In this section, we will show that this model can achieve the conditions needed to explain the gamma ray excess in the Galactic Center region. In order to calculate the dark matter cross section, we need the interactions between Higgs and fermions:

$$\begin{aligned}\mathcal{L} \supset & -\frac{\kappa_s}{\sqrt{2}}\left[h_s\bar{\tilde{s}}\tilde{s} - ia_s\bar{\tilde{s}}\gamma^5\tilde{s}\right] \\ & -\frac{\kappa_q}{2\sqrt{2}}\left[h_u\bar{\tilde{s}}\tilde{h}_d - ia_u\bar{\tilde{s}}\gamma^5\tilde{h}_d + h_d\bar{\tilde{s}}\tilde{h}_u - ia_d\bar{\tilde{s}}\gamma^5\tilde{h}_u + h.c.\right] \\ & -\frac{\kappa_\ell}{2\sqrt{2}}\left[h_0\bar{\tilde{s}}\tilde{h}_\ell - ia_0\bar{\tilde{s}}\gamma^5\tilde{h}_\ell + h_\ell\bar{\tilde{s}}\tilde{h}_0 - ia_\ell\bar{\tilde{s}}\gamma^5\tilde{h}_0 + h.c.\right] \\ & -\sum_{f=\{u,d,\ell\}}\sum_j \frac{m_{f_j}}{v_f}\left(h_f\bar{f}_jf_j - ia_f\bar{f}_j\gamma^5 f_j\right),\end{aligned} \tag{3.1}$$

where m_{f_j} is the mass of the fermion f_j, v_f is the vev of f-type scalars, and j runs over the fermion generations. In the limit $\kappa_q, \kappa_\ell \to 0$, the higgs-higgsino-singlino interactions vanish.

We can expand $\langle\sigma v\rangle$ in powers of the dark matter velocity squared v^2:

$$\langle\sigma v\rangle = a + bv^2 + \ldots. \tag{3.2}$$

Only the s-wave contribution to a is relevant in discussing the gamma ray excess coming from dark matter annihilation since the velocity of the dark matter in the Galactic Center region is relatively low. An exception to this is within the sphere of influence of the Milky Way supermassive black hole, but this region corresponds to only a fraction of an arc second and is below FGST accuracy. As we see later, a_1 is mostly singlet for benchmark points A and B. Therefore the s-wave contribution to dark matter annihilation to fermions comes mostly from the s-channel diagram involving an exchange of the lightest pseudoscalar a_1

given in Fig. 1. It is approximately given by

$$a \;\approx\; \frac{N_c \kappa_s^2\, U_{1f}^2}{4\pi} \frac{m_f^2}{v_f^2} \frac{m_{\chi_1}^2}{(4m_{\chi_1}^2 - m_{a_1}^2)^2} \sqrt{1 - \frac{m_f^2}{m_{\chi_1}^2}}, \tag{3.3}$$

where N_c is the number of fermion colors, U_{1f} is the $(1, f)$ element of the pseudoscalar diagonalizing matrix and m_{a_1} is the mass of the lightest pseudoscalar. The s-wave contributions from heavier pseudoscalars are suppressed by larger masses as well as smaller mixings with the singlet. Moreover, s-channel scalar exchange diagrams are s-wave suppressed, i.e. $a\,(\chi_1\chi_1 \to h_i \to \bar{f}f) = 0$.

For benchmark point A, the dark matter mass is $m_{\chi_1} = 7.4$ GeV. The physical dark matter can be expressed in terms of gauge eigenstates as:

$$\chi_1 = 0.0017\,\widetilde{B}^0 - 0.0031\,\widetilde{W}^0 - 0.0141\,\tilde{h}_u - 0.0046\,\tilde{h}_d - 0.0001\,\tilde{h}_0 - 0.0008\,\tilde{h}_\ell + 0.9999\,\tilde{s}.$$

We need a light pseudoscalar, $\mathcal{O}(10)$ GeV, to get a sizeable annihilation cross section. This requires 1% tuning in the parameter space in addition to the tuning needed to make the singlino the LSP. The lightest pseudoscalar in the benchmark point is mostly singlet with a mixing with other types of pseudoscalar given by

$$a_1 = -0.000002\,a_u - 0.002193\,a_d - 0.001203\,a_0 - 0.003679\,a_\ell + 0.999990\,a_s,$$

with its mass is $m_{a_1} = 18.7$ GeV.

Having the masses and mixing, we can calculate the total annihilation cross section into fermion pairs which gives

$$\langle \sigma v \rangle \;=\; 4.0 \times 10^{-26}\ \mathrm{cm}^3/\mathrm{s} \tag{3.4}$$

where the hadronic final states cross section is 23% of the total cross section and τ pairs final state makes up the rest. For benchmark point B given in Table II, the mass of dark matter is $m_{\chi_1} = 7.4$ GeV and $\langle \sigma v \rangle = 3.0 \times 10^{-26}$ cm^3/s, with the hadronic final states make up 23% of it. The annihillation cross sections given above are within the range of suggested cross section for explaining the gamma ray excess in the Galactic Center region given in Ref. [1].

In this model, dark matter annihilation into SM fermions given in Fig. 1 is also responsible for giving the dark matter the correct thermal relic abundance. To show this, we calculate the relic abundance which is given by [16]

$$\Omega_{\chi_1} h^2 \approx 2.82 \times 10^8\, Y_\infty (m_{\chi_1}/\mathrm{GeV}), \tag{3.5}$$

where

$$Y_\infty^{-1} = 0.264\,\sqrt{g_*} m_P m_{\chi_1} \left\{ a/x_f + 3(b - \tfrac{1}{4}a)/x_f^2 \right\}. \tag{3.6}$$

In the equation above, m_P is the Planck mass and g_* is the number of relativistic degrees of freedom at freeze-out. The freeze-out epoch x_f is related to the freeze-out temperature T_f by $x_f = m_{\chi_1}/T_f$, and x_f is determined by [16]

$$x_f = \ln\left[0.0764\, m_P (a + 6b/x_f) c(2+c) m_{\chi_1}/\sqrt{g_* x_f}\right]. \tag{3.7}$$

The value of c is usually taken as $c = \frac{1}{2}$. Approximating g_* to be a ladder function, we get that, for both of our benchmark points, the freeze-out epoch is $x_f = 21$ and the relic abundance is

$$\Omega_{\chi_1} h^2 \approx 0.1, \tag{3.8}$$

which agrees with the cosmologically measured abundance [17]. Since the freeze-out temperature happens to be around the QCD phase transition temperature, g_* varies significantly over the change of temperature [18] and the result (3.8) can change up to $\mathcal{O}(1)$. However the relic density is in the correct ballpark, therefore we do not expect that the correction will invalidate our result. An adjustment of parameters can be done when taking into account of the variation of g_* to get the correct density and annihilation cross section.

The benchmark points A and B serve as examples to show that in principle this model can explain the gamma ray excess in the Galactic Center region. However, the excess could also be obtained by some other regions in the parameter space as shown in the Appendix B. One could do a scan on the parameter space to find the favored region of the model.

Note that in our relic density calculation, we have neglected possible chargino and sfermion contributions coming from resonance and coannihilation effects. This is because the charginos have masses $\mathcal{O}(100)$ GeV for all of our benchmark points, and we assume that the sfermion masses are at least $\mathcal{O}(100)$ GeV, which is consistent with current LEP bounds.

IV. DIRECT DETECTION

Having shown that this model can account for the gamma ray excess in the Galactic Center region, we now discuss direct detection of dark matter of this model. In this section, we will consider constraints from the search for spin independent, elastic scattering of dark

matter off target nuclei. The most relevant contribution for the cross section is given by the t-channel scalar exchange diagram with the effective Lagrangian:

$$\mathcal{L}_{int} = \sum_q \alpha_q \bar{\chi}_1 \chi_1 \bar{q} q. \tag{4.1}$$

In our benchmark points, the only relevant contribution to dark matter detection comes from the lightest scalar and α_q can be approximated by

$$\alpha_q \approx \frac{\kappa_s m_q V_{1q}}{\sqrt{2} v_q m_{h_1}^2}, \tag{4.2}$$

where m_q is the mass of quark q, v_q is the scalar vev associated with quark flavor q, V_{1q} is the $(1, q)$ element of the scalar diagonalizing matrix, and m_{h_1} is the mass of the lightest scalar. Given the partonic interaction between dark matter and quarks, we can follow Ref. [19] to get the effective interaction with nucleons:

$$\mathcal{L}_{eff} = f_p \, \bar{\chi}_1 \chi_1 \, \bar{p} p + f_n \, \bar{\chi}_1 \chi_1 \, \bar{n} n, \tag{4.3}$$

where f_p and f_n are related to α_q through the relation [19]

$$\frac{f_{p,n}}{m_{p,n}} = \sum_{q=u,d,s} \frac{f_{Tq}^{(p,n)} \alpha_q}{m_q} + \frac{2}{27} f_{Tg}^{(p,n)} \sum_{q=c,b,t} \frac{\alpha_q}{m_q}, \tag{4.4}$$

and $\langle n | m_q \bar{q} q | n \rangle = m_n f_{Tq}^n$. Numerically, the $f_{Tq}^{(p,n)}$ are given by [20]

$$\begin{aligned} f_{Tu}^p = 0.020 \pm 0.004, \, f_{Td}^p = 0.026 \pm 0.005, \; f_{Ts}^p = 0.118 \pm 0.062 \\ f_{Tu}^n = 0.014 \pm 0.0043, \, f_{Td}^n = 0.036 \pm 0.008, \; f_{Ts}^n = 0.118 \pm 0.062, \end{aligned} \tag{4.5}$$

while $f_{Tg}^{(p,n)}$ is defined by

$$f_{Tg}^{(p,n)} = 1 - \sum_{q=u,d,s} f_{Tq}^{(p,n)} \; . \tag{4.6}$$

We can approximate $f_p \approx f_n$ since f_{Ts} is larger than other f_{Tq}'s and f_{Tg}. For the purpose of comparing the predicted cross section with existing bounds, we evaluate the cross section for scattering off a single nucleon. The result can be approximated as

$$\sigma_{SI} \approx \frac{4 m_r^2 f_p^2}{\pi} \tag{4.7}$$

where m_r is nucleon-dark matter reduced mass $1/m_r = 1/m_n + 1/m_{\chi_1}$.

We are now ready to show that benchmark point A can explain signals reported by CoGeNT [9] and DAMA [10]. For this benchmark point, the lightest scalar mass is $m_{h_1} = 11.3$ GeV. This lightest scalar is mostly singlet and its mixing with other scalars is given by

$$h_1 = 0.089\, h_u + 0.004\, h_d + 0.010\, h_0 + 0.004\, h_\ell + 0.996\, h_s.$$

As in the case of pseudoscalar, contributions from higher mass scalars are suppressed by their masses and their mixings with the singlet. The spin independent cross section for the benchmark point now can be calculated and is given by

$$\sigma_{SI} = 1.7 \times 10^{-40}\ \text{cm}^2, \tag{4.8}$$

which is inside the CoGeNT and DAMA favored region [11].

Similarly, we can show that benchmark point B given in Table II has the lightest scalar mass $m_{h_1} = 41.5$ GeV and spin independent cross section $\sigma_{SI} = 1.2 \times 10^{-42}$ cm^2. This cross section is two orders of magnitude lower than the present CDMS and XENON bound [12, 13].

V. BOUNDS ON THE MODEL

In this section we discuss various collider bounds that apply to the model. We will spend most of the discussions in this section for the benchmark point A given in Table I. The bounds for benchmark point B as well as the summary of the bounds for benchmark point A are given in Table III.

In this model, the decays $Z \to \chi_1\chi_1$ and $Z \to h_1 a_1$ are allowed kinematically. The Z decay width has been measured precisely and is given by $\Gamma = 2.4952 \pm 0.0023$ GeV [21]. Corrections to the decay width can be used as a bound on the mixing between the singlet and the Higgs sector. The partial decay width of $Z \to \chi_1\chi_1$ is given by

$$\Gamma_{Z\to\chi_1\chi_1} = \frac{G_F\theta_\chi^2}{48\sqrt{2}\pi} m_Z^3 \left(1 - \frac{4m_{\chi_1}^2}{m_Z^2}\right)^{\frac{3}{2}}, \tag{5.1}$$

where G_F is the Fermi constant, m_Z is Z mass, and θ_χ is given by

$$\theta_\chi = |W_{u1}|^2 - |W_{d1}|^2 + |W_{01}|^2 - |W_{\ell 1}|^2\,. \tag{5.2}$$

Benchmark point	A	B
m_{χ_1} (GeV)	7.4	7.4
$m_{\chi_1^\pm}$ (GeV)	118	118
m_{h_1} (GeV)	11.3	41.5
m_{a_1} (GeV)	18.7	19.3
$\Gamma_{Z\to\chi_1\chi_1}$ (GeV)	1.4×10^{-9}	1.4×10^{-9}
$\Gamma_{Z\to h_1a_1}$ (GeV)	1.1×10^{-11}	4.9×10^{-12}
k	8.0×10^{-3}	1.3×10^{-2}
$S_{model}(e^+e^-\to h_1a_1)$	1×10^{-10}	1×10^{-10}
$S_{model}(e^+e^-\to h_2a_1)$	1×10^{-12}	2×10^{-12}
$\sigma_{e^+e^-\to\chi_1\chi_2}$ (pb)	1×10^{-5}	1×10^{-5}

TABLE III: Mass spectrum and bounds for benchmark points A and B. The variable k is given by $k=\sigma_{hZ}/\sigma_{hZ}^{SM}$ and $S_{model}=\sigma_{h_ia_j}/\sigma_{ref}$, where $\sigma_{h_ia_j}$ is the h_ia_j production cross section and σ_{ref} is the reference cross section defined in Ref. [23].

In the equation above, W_{f1} is the $(f,1)$ element of the neutralino diagonalizing matrix. The decay width of $Z\to h_1a_1$ is given by

$$\Gamma_{Z\to h_1a_1}=\frac{G_F|\theta_{ha}|^2}{3\sqrt{2}\pi}p^3, \tag{5.3}$$

where

$$\theta_{ha}=U_{u1}V_{u1}-U_{d1}V_{d1}+U_{01}V_{01}-U_{\ell1}V_{\ell1}, \tag{5.4}$$

and

$$p^2=\frac{1}{4m_Z^2}\left[\left(m_Z^2-(m_{h_1}+m_{a_1})^2\right)\left(m_Z^2-(m_{h_1}-m_{a_1})^2\right)\right]. \tag{5.5}$$

For the benchmark point, the partial decay widths in both cases are given by

$$\begin{aligned}\Gamma_{Z\to\chi_1\chi_1}&=1.4\times10^{-9}\text{ GeV},\\ \Gamma_{Z\to h_1a_1}&=1.1\times10^{-11}\text{ GeV},\end{aligned} \tag{5.6}$$

which is well within the measurement error.

Another bound on the model comes from scalar and pseudoscalar direct production at LEP. At LEP a light scalar can be produced by Higgsstrahlung process $e^+e^-\to Z\to Zh_1$.

Ref. [22] gives a bound on the coupling strength of Z pairs to scalars regardless of the scalar's decay mode. The bound is given in terms of the quantity

$$k(m_h) = \frac{\sigma_{hZ}}{\sigma_{hZ}^{SM}}. \tag{5.7}$$

In our model, $k(m_h)$ is given by

$$k(m_{h_i}) = \frac{1}{v_{\rm ew}^2} \left| v_u V_{ui} + v_d V_{di} + v_0 V_{0i} + v_\ell V_{\ell i} \right|^2, \tag{5.8}$$

and its value for the lightest scalar at our benchmark point is

$$k(m_{h_1}) = 8.0 \times 10^{-3}. \tag{5.9}$$

The bound on $k(m_h)$ for the benchmark point h_1 mass is given by

$$k(11.3 \text{ GeV}) \leq 0.09. \tag{5.10}$$

Therefore $k(m_{h_1})$ does not exceed the bound from Higgsstrahlung process in our benchmark point. The pseudoscalar can also be produced at LEP by the process $e^+e^- \to Z \to ha$. In the benchmark point, both h_1a_1 and h_2a_1 production are kinematically allowed. LEP bounds on scalar and pseudoscalar production for various final states are given in Ref. [23]. The bound is given in term of $S_{95} = \sigma_{max}/\sigma_{ref}$ where σ_{max} is the largest cross section compatible with data and σ_{ref} is the standard model hZ production cross section multiplied by a kinematic scaling factor. Defining $S_{model} = \sigma_{h_ia_j}/\sigma_{ref}$, where $\sigma_{h_ia_j}$ is the model's h_ia_j production cross section, the bound on the model is given by $S_{model} < S_{95}$. For our benchmark point, S_{model} is given by

$$\begin{aligned} S_{model}(e^+e^- \to h_1a_1) &= 1 \times 10^{-10}, \\ S_{model}(e^+e^- \to h_2a_1) &= 1 \times 10^{-12}, \end{aligned} \tag{5.11}$$

which is lower than the bound, $S_{95} \sim \mathcal{O}(10^{-2})$, in both cases.

We note that the lightest chargino mass is 118 GeV for the benchmark point, which exceeds the PDG bound of 94 GeV [21]. In the case of a long lived chargino however, the bound can be made much stronger and is currently at 171 GeV. We have calculated the lifetime of the chargino in our model assuming a stau mass of 110 GeV and have found that it is short lived, thus this latter bound is not of concern. We should point out however, that our analysis has been done at tree level. Loop corrections could change these results but are beyond the scope of this paper.

Finally, we need to calculate the bound on neutralino productions. Ref. [24] discusses the bound on production of the lightest and second to lightest neutralinos at LEP, $e^+e^- \to \chi_1\chi_2$, where χ_2 decays into $\chi_1 f\bar{f}$. Assuming that the selectron is much heavier than the Z, the main contribution comes from s-channel Z exchange. For our benchmark point, we calculate the cross section to be

$$\sigma_{e^+e^-\to\chi_1\chi_2} = 1 \times 10^{-5} \text{ pb}, \tag{5.12}$$

while the bound is $\mathcal{O}(0.1)$ pb. A summary of all these bounds is given in Table III.

The light particles are mostly singlet and have very little mixing with the Higgs sector. This make the particles unlikely to be produced at near future experiments. However the heavier sector has a richer phenomenology. For example, heavier scalars are mostly h_u, h_d, h_0, and h_ℓ therefore they have a better chance of being detected in future colliders [6].

VI. CONCLUSIONS

In this paper, we have presented a supersymmetric model of $7-10$ GeV dark matter, which is capable of describing the FGST observations. In a recent analysis of FGST data, Hooper and Goodenough found an excess in gamma ray emission from within 1.25° of the Galactic Center. They showed that this can be explained by annihilating dark matter if the dark matter has a mass between $7-10$ GeV, annihilates into τ-pairs most of the time, but into hadronic channels the other $15-40\%$ of the time, and $\langle\sigma v\rangle$ falls within the range $4.6\times10^{-27} - 5.3\times10^{-26}$ cm^3/s [1]. Our model achieves these requirements by minimally extending the SLHM to include a scalar singlet whose superpartner is the dark matter particle. Due to the Yukawa structure of the SLHM the scalar particles mediating the dark matter annihilation have an enhanced coupling to leptons. This provides a natural means for satisfying the second requirement put forward by Hooper and Goodenough.

We have shown that this model produces the correct dark matter thermal relic density and is consistent with current collider bounds. In addition, we have shown that this model is consistent with the direct detection signals reported by both CoGeNT and DAMA for certain regions of parameter space, while for other regions of parameter space, the model yields a spin independent cross section far below the present CDMS bound, but maintains the right relic density and continues to explain the FGST observations. Thus our model is fully able to accommodate the results reported by CoGeNT and DAMA in the case of their

Field	$\mathbb{Z}_{3q}$	$\mathbb{Z}_{3\ell}$	Field	$\mathbb{Z}_{3q}$	$\mathbb{Z}_{3\ell}$
$\widehat{H}_u$	ω	1	$\widehat{X}_{01}$	1	1
$\widehat{H}_d$	ω	1	$\widehat{X}_{02}$	ω^2	ω^2
$\widehat{H}_0$	1	ω	$\widehat{X}_{q1}$	ω	1
$\widehat{H}_\ell$	1	ω	$\widehat{X}_{q2}$	ω^2	1
$\widehat{E}$	1	ω^2	$\widehat{X}_{\ell 1}$	1	ω
$\widehat{Q}$	ω^2	1	$\widehat{X}_{\ell 2}$	1	ω^2

TABLE IV: Transformation rule for the $\mathbb{Z}_{3q} \times \mathbb{Z}_{3\ell}$ symmetry. Each field transforms as $\phi \to X\phi$, where X is the corresponding factor shown in the table. For each case, $\omega^3 = 1$. Other fields not shown in the table are neutral under $\mathbb{Z}_{3q} \times \mathbb{Z}_{3\ell}$

vindication, but it is in no way contingent upon their validity.

Acknowledgments

We thank Chris Carone and Marc Sher for useful discussions and their many comments on this manuscript. We also thank Dylan Albrecht for comments on this manuscript. This work was supported by the NSF under Grant PHY-0757481.

Appendix A: Breaking Terms

In this appendix, we discuss a possible source of the terms in V_{soft} that break the $\mathbb{Z}_2$ symmetry of the superpotential. Generally, one can imagine such breaking terms arising from the F-term of some hidden sector superfield receiving a vacuum expectation value. To be more specific, we consider a possible scenario that results in such breaking terms and also explains the smallness of κ_q and κ_ℓ. In this scenario there is a hidden sector, which contains the six fields $\widehat{X}_{01}$, $\widehat{X}_{02}$, $\widehat{X}_{q1}$, $\widehat{X}_{q2}$, $\widehat{X}_{\ell 1}$ and $\widehat{X}_{\ell 2}$. The F-terms of the fields receive vevs

$$\langle F_{X_i} \rangle \sim \mathcal{O}(10^{11}\text{GeV})^2, \tag{A1}$$

so that

$$M_{\text{SUSY}} \sim \frac{\langle F_{X_i} \rangle}{M_P} \tag{A2}$$

is at the TeV scale. The index i denotes 01, 02, $q1$, $q2$, $\ell 1$, and $\ell 2$. A $\mathbb{Z}_{3q} \times \mathbb{Z}_{3\ell}$ symmetry is imposed, under which the fields transform according to Table IV. The hidden sector fields $\widehat{X}_i$ couple to visible sector fields in a high energy, fundamental theory, and are Planck suppressed in the low energy effective theory. Consequentially, the lagrangian contains terms such as

$$\Delta\mathcal{L} = \frac{f'}{M_P^2}\int d^4\theta \widehat{X}_{01}^\dagger \widehat{X}_{02}\widehat{H}_u\widehat{H}_\ell + \frac{m'}{M_P}\int d^2\theta \widehat{X}_{02}\widehat{S}\widehat{H}_u\widehat{H}_\ell + \text{h.c.}, \tag{A3}$$

where $d^2\theta = d(\theta\theta)$ and $d^4\theta = d(\theta\theta)d(\bar{\theta}\bar{\theta})$ represent integration over Grassmann variables and f' and m' are coupling constants. When the F-terms of $\widehat{X}_{01}$ and $\widehat{X}_{02}$ receive vevs, the terms in Eq. (A3) give rise to

$$\begin{aligned}\Delta\mathcal{L} &= \frac{f'\langle F_{01}\rangle\langle F_{02}\rangle}{M_P^2}\int d^4\theta(\bar{\theta}\bar{\theta})(\theta\theta)\widehat{H}_u\widehat{H}_\ell + \frac{m'\langle F_{02}\rangle}{M_P}\int d^2\theta(\theta\theta)\widehat{S}\widehat{H}_u\widehat{H}_\ell + \text{h.c.}\\ &= \frac{f'\langle F_{01}\rangle\langle F_{02}\rangle}{M_P^2}H_uH_\ell + \frac{m'\langle F_{02}\rangle}{M_P}SH_uH_\ell + \text{h.c.}\\ &\to \mu_3^2 H_uH_\ell + \mu_c SH_uH_\ell + \text{h.c.}.\end{aligned} \tag{A4}$$

Similarly, the breaking parameters μ_4^2 and μ_d arise from the Planck suppressed terms

$$\begin{aligned}\Delta\mathcal{L} &= \frac{g'}{M_P^2}\int d^4\theta \widehat{X}_{01}^\dagger \widehat{X}_{02}\widehat{H}_0\widehat{H}_d + \frac{n'}{M_P}\int d^2\theta \widehat{X}_{02}\widehat{S}\widehat{H}_0\widehat{H}_d + \text{h.c.}\\ &\to \frac{g'\langle F_{01}\rangle\langle F_{02}\rangle}{M_P^2}H_0H_d + \frac{n'\langle F_{02}\rangle}{M_P}SH_0H_d + \text{h.c.}\\ &\to \mu_4^2 H_0H_d + \mu_d SH_0H_d + \text{h.c.},\end{aligned} \tag{A5}$$

while the parameters m_{u0}^2 and $m_{d\ell}^2$ arise from

$$\begin{aligned}\Delta\mathcal{L} &= \frac{h'}{M_P^2}\int d^4\theta \widehat{X}_{02}^\dagger \widehat{X}_{\ell 1}\widehat{H}_u^\dagger\widehat{H}_0 + \frac{i'}{M_P^2}\int d^4\theta \widehat{X}_{02}^\dagger \widehat{X}_{\ell 1}\widehat{H}_d^\dagger\widehat{H}_\ell + \text{h.c.}\\ &\to \frac{h'\langle F_{02}\rangle\langle F_{\ell 1}\rangle}{M_P^2}H_u^\dagger H_0 + \frac{i'\langle F_{02}\rangle\langle F_{\ell 1}\rangle}{M_P^2}H_d^\dagger H_\ell + \text{h.c.}\\ &\to m_{u0}^2 H_u^\dagger H_0 + m_{d\ell}^2 H_d^\dagger H_\ell + \text{h.c.}.\end{aligned} \tag{A6}$$

In this way, all of the $\mathbb{Z}_2$ breaking terms are generated. At this point it should be noted that the $\mathbb{Z}_{3q} \times \mathbb{Z}_{3\ell}$ symmetry actually prohibits the terms $\mu_q\hat{H}_u\hat{H}_d$, $\mu_\ell\hat{H}_0\hat{H}_\ell$, $\kappa_q\hat{S}\hat{H}_u\hat{H}_d$, and $\kappa_\ell\hat{S}\hat{H}_0\hat{H}_\ell$ from appearing in the superpotential [see Eq. (2.1)]. As far as the μ_q and μ_ℓ terms are concerned, this is not a problem since they are generated by the vevs of the $\widehat{X}_{q2}$ and $\widehat{X}_{\ell 2}$

$\frac{a'}{M_P}\int d^4\theta \widehat{X}_{q2}^\dagger \widehat{H}_u \widehat{H}_d + \text{h.c.}$	$\int d^2\theta \mu_q \widehat{H}_u \widehat{H}_d + \text{h.c.}$
$\frac{b'}{M_P}\int d^4\theta \widehat{X}_{\ell 2}^\dagger \widehat{H}_0 \widehat{H}_l + \text{h.c.}$	$\int d^2\theta \mu_\ell \widehat{H}_0 \widehat{H}_\ell + \text{h.c.}$
$\frac{c'}{M_P}\int d^4\theta \widehat{X}_{01}^\dagger \widehat{S}^2 + \text{h.c.}$	$\int d^2\theta \lambda_2 \widehat{S}^2 + \text{h.c.}$
$\frac{1}{M_P^2}\int d^4\theta \left(d' \widehat{X}_{01}^\dagger \widehat{X}_{q1} + d'' \widehat{X}_{q2}^\dagger \widehat{X}_{01} + d''' \widehat{X}_{02}^\dagger \widehat{X}_{\ell 2} + d'''' \widehat{X}_{q1}^\dagger \widehat{X}_{q2}\right) \widehat{H}_u \widehat{H}_d + \text{h.c.}$	$\mu_1^2 H_u H_d + \text{h.c.}$
$\frac{1}{M_P^2}\int d^4\theta \left(e' \widehat{X}_{01}^\dagger \widehat{X}_{\ell 1} + e'' \widehat{X}_{\ell 2}^\dagger \widehat{X}_{01} + e''' \widehat{X}_{02}^\dagger \widehat{X}_{q2} + e'''' \widehat{X}_{\ell 1}^\dagger \widehat{X}_{\ell 2}\right) \widehat{H}_0 \widehat{H}_\ell + \text{h.c.}$	$\mu_2^2 H_0 H_\ell + \text{h.c.}$
$\frac{1}{M_P^2}\int d^4\theta \left(f' \widehat{X}_{01}^\dagger \widehat{X}_{02} + f'' \widehat{X}_{q1}^\dagger \widehat{X}_{\ell 2} + f''' \widehat{X}_{\ell 1}^\dagger \widehat{X}_{q2}\right) \widehat{H}_u \widehat{H}_\ell + \text{h.c.}$	$\mu_3^2 H_u H_\ell + \text{h.c.}$
$\frac{1}{M_P^2}\int d^4\theta \left(g' \widehat{X}_{01}^\dagger \widehat{X}_{02} + g'' \widehat{X}_{q1}^\dagger \widehat{X}_{\ell 2} + g''' \widehat{X}_{\ell 1}^\dagger \widehat{X}_{q2}\right) \widehat{H}_0 \widehat{H}_d + \text{h.c.}$	$\mu_4^2 H_0 H_d + \text{h.c.}$
$\frac{1}{M_P^2}\int d^4\theta \left(h' \widehat{X}_{02}^\dagger \widehat{X}_{\ell 1} + h'' \widehat{X}_{q1}^\dagger \widehat{X}_{02} + h''' \widehat{X}_{q2}^\dagger \widehat{X}_{\ell 2} + h'''' \widehat{X}_{\ell 1}^\dagger \widehat{X}_{q1}\right) \widehat{H}_u^\dagger \widehat{H}_0 + \text{h.c.}$	$m_{u0}^2 H_u^\dagger H_0 + \text{h.c.}$
$\frac{1}{M_P^2}\int d^4\theta \left(i' \widehat{X}_{02}^\dagger \widehat{X}_{\ell 1} + i'' \widehat{X}_{q1}^\dagger \widehat{X}_{02} + i''' \widehat{X}_{q2}^\dagger \widehat{X}_{\ell 2} + i'''' \widehat{X}_{\ell 1}^\dagger \widehat{X}_{q1}\right) \widehat{H}_d^\dagger \widehat{H}_\ell + \text{h.c.}$	$m_{d\ell}^2 H_d^\dagger H_\ell + \text{h.c.}$
$\frac{1}{M_P^2}\int d^4\theta \sum_i j^i \widehat{X}_i^\dagger \widehat{X}_i \widehat{H}_f^\dagger \widehat{H}_f + \text{h.c.}$	$m_f^2 \lvert H_f\rvert^2 + \text{h.c.}$
$\frac{k'}{M_P}\int d^2\theta \widehat{X}_{q1} \widehat{S} \widehat{H}_u \widehat{H}_d + \text{h.c.}$	$\mu_a S H_u H_d + \text{h.c.}$
$\frac{l'}{M_P}\int d^2\theta \widehat{X}_{\ell 1} \widehat{S} \widehat{H}_0 \widehat{H}_\ell + \text{h.c.}$	$\mu_b S H_0 H_\ell + \text{h.c.}$
$\frac{m'}{M_P}\int d^2\theta \widehat{X}_{02} \widehat{S} \widehat{H}_u \widehat{H}_\ell + \text{h.c.}$	$\mu_c S H_u H_\ell + \text{h.c.}$
$\frac{n'}{M_P}\int d^2\theta \widehat{X}_{02} \widehat{S} \widehat{H}_0 \widehat{H}_d + \text{h.c.}$	$\mu_d S H_0 H_d + \text{h.c.}$
$\frac{1}{M_P^2}\int d^4\theta \sum_i o^i \widehat{X}_i^\dagger \widehat{X}_i \widehat{S}^2 + \text{h.c.}$	$b_s^2 S^2 + \text{h.c.}$
$\frac{p'}{M_P}\int d^2\theta \widehat{X}_0 \widehat{S}^3 + \text{h.c.}$	$a_s S^3 + \text{h.c.}$

TABLE V: A complete list of superpotential and V_{soft} terms generated by the X_i in this example.

fields in the same manner:

$$\begin{aligned}
\Delta\mathcal{L} &= \frac{a'}{M_P}\int d^4\theta \widehat{X}_{q2}^\dagger \widehat{H}_u \widehat{H}_d + \frac{b'}{M_P}\int d^4\theta \widehat{X}_{\ell 2}^\dagger \widehat{H}_0 \widehat{H}_\ell \\
&\to \frac{a'\langle F_{q2}\rangle}{M_P}\int d^2\theta d^2\bar\theta\,(\bar\theta\bar\theta)\widehat{H}_u \widehat{H}_d + \frac{b'\langle F_{\ell 2}\rangle}{M_P}\int d^2\theta d^2\bar\theta\,(\bar\theta\bar\theta)\widehat{H}_0 \widehat{H}_\ell \\
&= \frac{a'\langle F_{q2}\rangle}{M_P}\int d^2\theta \widehat{H}_u \widehat{H}_d + \frac{b'\langle F_{\ell 2}\rangle}{M_P}\int d^2\theta \widehat{H}_0 \widehat{H}_\ell \\
&\to \mu_q \int d^2\theta \widehat{H}_u \widehat{H}_d + \mu_\ell \int d^2\theta \widehat{H}_0 \widehat{H}_\ell .
\end{aligned} \tag{A7}$$

In this UV completion scenario, the terms corresponding to κ_q, κ_ℓ, λ_1 and t are not generated in this way. Because of the $\mathbb{Z}_{3q} \times \mathbb{Z}_{3\ell}$ symmetry, they are entirely absent at tree level. Benchmark points II and V in Table VI satisfy $\kappa_q = \kappa_\ell = \lambda_1 = t = 0$ and yield results consistent with our goals. Since we are not committing to this particular UV completion scheme, we consider several other benchmark points that include nonzero values for these parameters. A list of the soft breaking terms relevant to this paper, which are generated by

the fields X_i, is given in Table V.

Appendix B: List of benchmark points

In this Appendix, we show several benchmark points given in Table VI. Benchmarks point I-III lie in the suggested CoGeNT and DAMA range, while benchmarks point IV-VI satisfy CDMS bound. Benchmark point I is identical with benchmark point A discussed in the text. Benchmark point IV is identical with benchmark point B. Benchmark points II and V are motivated by mechanism described in Appendix A.

TABLE VI: Additional benchmark points

Benchmark point	I	II	III	IV	V	VI
κ_q	0.01	0	0.01	0.01	0	0.01
κ_l	0.01	0	0.01	0.01	0	0.01
κ_s	0.6	0.6	0.5	0.6	0.6	0.5
$\tan\alpha$	20	15	30	20	30	25
$\tan\beta$	50	30	30	50	25	25
$\tan\beta_\ell$	10	10	5	10	5	5
v_s (GeV)	50	50	100	50	50	100
v_u (GeV)	245.6	245.3	245.7	245.6	245.7	245.6
v_d (GeV)	4.9	8.2	8.2	4.9	9.8	9.8
v_0 (GeV)	12.2	16.2	8.0	12.2	8.0	9.6
v_ℓ (GeV)	1.2	1.6	1.6	1.2	1.6	1.9
μ_q (GeV)	125	125	200	125	125	150
μ_ℓ (GeV)	125	125	150	125	150	150
λ_1^2 (GeV^2)	100^2	0	150^2	100^2	0	50^2
λ_2 (GeV)	-35	-35	-63	-35	-35	-63
M_1 (GeV)	500	500	250	500	250	200
M_2 (GeV)	500	500	500	500	500	400
m_{u0}^2 (GeV^2)	-100^2	-150^2	-150^2	-100^2	-150^2	-150^2
$m_{d\ell}^2$ (GeV^2)	100^2	200^2	100^2	100^2	200^2	100^2
μ_1^2 (GeV^2)	400^2	300^2	300^2	400^2	400^2	350^2
μ_2^2 (GeV^2)	200^2	300^2	250^2	200^2	200^2	300^2
μ_3^2 (GeV^2)	200^2	200^2	250^2	200^2	250^2	200^2
μ_4^2 (GeV^2)	400^2	200^2	200^2	400^2	400^2	100^2
μ_a (GeV)	100	75	75	100	100	80
μ_b (GeV)	200	150	300	200	250	400
μ_c (GeV)	200	200	400	200	300	200
μ_d (GeV)	200	100	100	200	250	100

Continued on the next page

TABLE VI: continued

Benchmark point	I	II	III	IV	V	VI
t^3 (GeV^3)	60.6^3	0	83.9^3	55.0^3	0	-87.9^3
b_s^2 (GeV^2)	63.4^2	43.6^2	98.2^2	66.3^2	47.1^2	99.0^2
a_s (GeV)	-42.4	-21.7	-50.2	-42.2	-20.0	-50.2
m_{χ_1} (GeV)	7.4	7.4	7.7	7.4	7.4	7.7
$m_{\chi_1^\pm}$ (GeV)	118	117	151	118	117	137
m_{h_1} (GeV)	11.3	19.2	12.8	41.5	41.4	23.1
m_{a_1} (GeV)	18.7	16.1	18.8	19.3	19.2	11.7
$\langle\sigma v\rangle$ ($\frac{\text{cm}^3}{\text{s}}$)	4.0×10^{-26}	3.4×10^{-26}	4.6×10^{-26}	3.0×10^{-26}	3.1×10^{-26}	4.1×10^{-26}
$\frac{\langle\sigma v\,(\chi_1\chi_1\to\text{hadrons})\rangle}{\langle\sigma v\rangle}$	23%	38%	32%	23%	24%	30%
σ_{SI}(cm^2)	1.7×10^{-40}	1.2×10^{-40}	1.5×10^{-40}	1.2×10^{-42}	6.1×10^{-42}	1.5×10^{-41}
$\Gamma_{Z\to\chi_1\chi_1}$ (GeV)	1.4×10^{-9}	0	2.1×10^{-10}	1.4×10^{-9}	0	6.3×10^{-10}
$\Gamma_{Z\to h_1a_1}$ (GeV)	1.1×10^{-11}	1.2×10^{-10}	1.4×10^{-10}	4.9×10^{-12}	4.2×10^{-11}	1.2×10^{-10}
k	8.0×10^{-3}	3.5×10^{-2}	2.2×10^{-2}	1.3×10^{-2}	0.12	2.8×10^{-2}
$S_{model}(e^+e^-\to h_1a_1)$	1×10^{-10}	2×10^{-9}	2×10^{-9}	1×10^{-10}	1×10^{-9}	2×10^{-9}
$S_{model}(e^+e^-\to h_2a_1)$	1×10^{-12}	5×10^{-11}	3×10^{-11}	2×10^{-12}	1×10^{-10}	4×10^{-11}
$\sigma_{e^+e^-\to\chi_1\chi_2}$ (pb)	1×10^{-5}	0	5×10^{-9}	1×10^{-5}	0	4×10^{-6}

[1] D. Hooper and L. Goodenough, Phys. Lett. B **697**, 412 (2011) [arXiv:1010.2752 [hep-ph]].

[2] A. Boyarsky, D. Malyshev and O. Ruchayskiy, arXiv:1012.5839 [hep-ph].

[3] K. N. Abazajian, arXiv:1011.4275 [astro-ph.HE].

[4] J. Kopp, V. Niro, T. Schwetz and J. Zupan, arXiv:1011.1398 [hep-ph]. M. R. Buckley, D. Hooper and T. M. P. Tait, arXiv:1011.1499 [hep-ph].; D. Hooper and T. Linden, arXiv:1011.4520 [astro-ph.HE].; K. N. Abazajian, S. Blanchet and J. P. Harding, arXiv:1011.5090 [hep-ph].; J. M. Siegal-Gaskins, R. Reesman, V. Pavlidou, S. Profumo and T. P. Walker, arXiv:1011.5501 [astro-ph.HE].; M. H. G. Tytgat, arXiv:1012.0576 [hep-ph]. K. N. Abazajian, S. Blanchet and J. P. Harding, arXiv:1012.1247 [astro-ph.CO].; A. Abada, S. Nasri and D. Ghaffor, arXiv:1101.0365 [hep-ph]. G. Zhu, arXiv:1101.4387 [hep-ph].

[5] C. Kelso and D. Hooper, arXiv:1011.3076 [hep-ph].

[6] G. Marshall and M. Sher, Phys. Rev. D **83**, 015005 (2011) [arXiv:1011.3016 [hep-ph]].

[7] H. S. Goh, L. J. Hall and P. Kumar, JHEP **0905**, 097 (2009) [arXiv:0902.0814 [hep-ph]].

[8] H. E. Logan, arXiv:1010.4214 [hep-ph]. V. Barger, Y. Gao, M. McCaskey and G. Shaughnessy, Phys. Rev. D **82**, 095011 (2010) [arXiv:1008.1796 [hep-ph]]. A. L. Fitzpatrick, D. Hooper and K. M. Zurek, Phys. Rev. D **81**, 115005 (2010) [arXiv:1003.0014 [hep-ph]]. A. R. Raklev and M. J. White, arXiv:0911.1986 [hep-ph].

[9] C. E. Aalseth *et al.* [CoGeNT Collaboration], [arXiv:1002.4703 [astro-ph.CO]].

[10] R. Bernabei *et al.* [DAMA Collaboration], Eur. Phys. J. **C56**, 333-355 (2008). [arXiv:0804.2741 [astro-ph]].; R. Bernabei *et al.*, Eur. Phys. J. C **67**, 39 (2010) [arXiv:1002.1028 [astro-ph.GA]].

[11] D. Hooper, J. I. Collar, J. Hall *et al.*, Phys. Rev. **D82**, 123509 (2010). [arXiv:1007.1005 [hep-ph]].

[12] E. Aprile *et al.* [XENON100 Collaboration], Phys. Rev. Lett. **105**, 131302 (2010) [arXiv:1005.0380 [astro-ph.CO]].

[13] Z. Ahmed *et al.* [CDMS-II Collaboration], arXiv:1011.2482 [astro-ph.CO].

[14] R. Kappl, M. Ratz and M. W. Winkler, Phys. Lett. B **695**, 169 (2011) [arXiv:1010.0553 [hep-ph]].

[15] J. Espinosa and M. Quirós, Phys. Lett. B **279**, 92 (1992); Phys. Lett. B **302**, 51 (1993).
G. Kane, C. Kolda and J. Wells, Phys. Rev. Lett. **70**, 2686 (1993).

[16] G. Jungman, M. Kamionkowski and K. Griest, Phys. Rept. **267**, 195 (1996) [arXiv:hep-ph/9506380].

[17] E. Komatsu *et al.* [WMAP Collaboration], Astrophys. J. Suppl. **180**, 330 (2009) [arXiv:0803.0547 [astro-ph]].

[18] P. Gondolo and G. Gelmini, Nucl. Phys. B **360**, 145 (1991).

[19] C. Munoz, Int. J. Mod. Phys. A **19**, 3093 (2004) [arXiv:hep-ph/0309346].

[20] J. R. Ellis, A. Ferstl and K. A. Olive, Phys. Lett. B **481**, 304 (2000) [arXiv:hep-ph/0001005].

[21] K. Nakamura *et al.* [Particle Data Group], J. Phys. G **37**, 075021 (2010).

[22] G. Abbiendi *et al.* [OPAL Collaboration], Eur. Phys. J. **C27**, 311-329 (2003). [hep-ex/0206022].

[23] S. Schael *et al.* [ALEPH and DELPHI and L3 and OPAL and LEP Working Group for Higgs

Boson Searches Collaborations], Eur. Phys. J. **C47**, 547-587 (2006). [hep-ex/0602042].

[24] J. Abdallah *et al.* [DELPHI Collaboration], Eur. Phys. J. C **31**, 421 (2003) [arXiv:hep-ex/0311019].